Ultrafast cooling by covalently bonded graphene-carbon nanotube hybrid immersed in water

Jie Chen[1,2], Jens H Walther[3,4] and Petros Koumoutsakos[4]

[1] Center for Phononics and Thermal Energy Science, School of Physics Science and Engineering, Tongji University, Shanghai 200092, People's Republic of China
[2] Institute for Advanced Study, Tongji University, Shanghai 200092, People's Republic of China
[3] Department of Mechanical Engineering, Technical University of Denmark, DK-2800 Kgs. Lyngby, Denmark
[4] Computational Science and Engineering Laboratory, Department of Mechanical and Process Engineering, ETH Zurich, CH-8092 Zurich, Switzerland

E-mail: jie@tongji.edu.cn and petros@ethz.ch

CrossMark

Abstract

The increasing power density and the decreasing dimensions of transistors present severe thermal challenges to the design of modern microprocessors. Furthermore, new technologies such as three-dimensional chip-stack architectures require novel cooling solutions for their thermal management. Here, we demonstrate, through transient heat-dissipation simulations, that a covalently bonded graphene-carbon nanotube (G-CNT) hybrid immersed in water is a promising solution for the ultrafast cooling of such high-temperature and high heat-flux surfaces. The G-CNT hybrid offers a unique platform to integrate the superior axial heat transfer capability of individual CNTs via their parallel arrangement. The immersion of the G-CNT in water enables an additional heat dissipation path via the solid–liquid interaction, allowing for the sustainable cooling of the hot surface under a constant power input of up to $10\,000\,W\,cm^{-2}$.

S Online supplementary data available from stacks.iop.org/NANO/27/465705/mmedia

Keywords: graphene, carbon nanotube, covalent bonding, liquid cooling, hotspot removal, molecular dynamics

(Some figures may appear in colour only in the online journal)

1. Introduction

Efficient thermal management is crucial for the performance of micro- and nano- electronic and optoelectronic devices [1]. A prominent example is the heat dissipation in integrated circuit (IC) chips, where the power density is in the order of $100\,W\,cm^{-2}$ for modern microprocessors [2]. Such high heat flux results in hotspots where the local temperature is significantly higher than the average chip temperature [3]. As the overall reliability is determined by the hottest region, these hotspots pose a severe thermal bottleneck for further size reduction in IC chips. Novel solutions at the package integration levels, such as three-dimensional (3D) chip stacking

[4], are emerging as a promising technology to enhance the computing performance without relying on the reduction of the feature size. The 3D stacking architectures have many advantages, such as shorter global-interconnect length, smaller chip footprint and heterogeneous integration. At the same time, the use of the third dimension in order to achieve such functionality comes at the price of elevated heat dissipation of up to $500\,W\,cm^{-2}$ in the 3D chips [5]. Hence, a high-performance cooling solution is indispensable for future nanoelectronics.

These extreme requirements for cooling of the IC have attracted researchers to the study of the remarkable thermal transport properties of graphene and carbon nanotubes

(CNTs) [6–32]. CNTs and single-layer graphene have intrinsically high thermal conductivity $\sim$3000 W m^{-1} K^{-1} at room temperature [6]. However, the large contact thermal resistance of CNTs and the low *c*-axis thermal conductivity in multilayer graphene present major roadblocks [28, 29] for their application as high-performance thermal interface materials (TIMs). Interestingly, a material that combines these two roadblocks has the potential to overcome them both. The covalently bonded graphene-CNT (G-CNT) hybrid, a recently synthesized structure [33, 34], has been found to have significantly enhanced *c*-axis thermal conductivity while providing a large surface contact for efficient heat transfer at the same time [35]. Consequently, the G-CNT hybrid outperforms both CNT and graphene in the *c*-axis heat transfer, and its thermal resistance is three orders of magnitude lower than the state-of-the-art TIMs [35].

The present study demonstrates that G-CNT is a promising TIM for cooling applications. We investigate the heat-dissipation performance of a G-CNT hybrid for cooling the high-temperature hot surface via non-equilibrium molecular dynamics (MD) simulation. We find the temperature of the hot surface decays exponentially with time, and the cooling performance is proportional to the number of CNTs arranged in parallel. Moreover, we demonstrate that by immersing the G-CNT hybrid in water, an additional heat-dissipation channel is established via the solid–liquid interaction, allowing for sustainable cooling of the hot surface under a constant power input of up to 10 000 W cm^{-2}. Our study provides novel insights into the thermal management of high power-density devices.

2. Structure and simulation details

As shown in figure 1, the G-CNT hybrid is seamlessly constructed by the sp^2 C-C bond at the junction [35]. Its two graphene layers offer planar contact with other surfaces, thus reducing the contact thermal resistance. Heat is transferred effectively through covalent bonding with the CNTs, leading to its ultrafast transport along their axes. The G-CNT hybrid is compatible with the next-generation 3D stacking of IC chips and can be used as the TIM between adjacent IC stacks. In this study, both the top and bottom graphene layers of the G-CNT are initially heated at high temperature to represent the hot surface, while the rest of the hybrid is kept at room temperature.

All MD simulations were performed using the LAMMPS package [36]. We employed the optimized Tersoff potential [37] to model the sp^2 bond in the G-CNT hybrid, and the flexible simple point-charge water model [38] with a time step of 0.5 fs. The water–carbon interaction is modeled by the Lennard–Jones (LJ) potential [39] and the Coulombic forces are computed by the particle–particle–particle–mesh (P^{3}M) method. After equilibrating the whole system at ambient temperature (300 K) with the NPT (isothermal–isobaric) ensemble, the hot surface is generated by applying high-temperature Langevin thermostats only to the top and bottom graphene layers while keeping the rest of the atoms frozen.

Finally, the thermostats are removed from the hot surface and the NVE (microcanonical) ensemble is used to simulate the transient heat-dissipation process. To model the infinitely large water reservoir (constant temperature), all the water molecules are equilibrated at ambient temperature with Langevin thermostats during the heat-dissipation process. We find that the CNT density is the dominant factor for the cooling performance (see supplementary information figure S1), instead of the cross-sectional area of graphene. Therefore, the cross-section of the top and bottom graphene is fixed at 6 nm $\times$ 5 nm throughout this study.

3. Results and discussions

Figure 2 shows the typical cooling process for the G-CNT hybrid in vacuum. Due to the high c-axis thermal conductivity of the G-CNT hybrid [35], the heat energy is rapidly evacuated from the graphene layers to the CNT, causing the exponential decay of the temperature for the two hot surfaces within tens of picoseconds (figure 2(a)). Compared to the multilayer graphene with the same thickness, G-CNT can speed up the cooling process by two orders of magnitude [35]. As the whole hybrid is an isolated system, its average temperature remains constant. The temperature profile in CNT reveals that the local temperature along the CNT length direction is highly non-uniform during the cooling process (figure 2(b)). At the beginning, except for the two ends that are covalently bonded to the hot surfaces, the majority of the CNT is still at initial (room) temperature. This room-temperature portion of the CNT acts as the heat sink (constant temperature) for absorbing the heat energy. As more heat is transmitted into the CNT, the heat sink keeps shrinking and eventually disappears after $\sim$5 ps. During this period, the hot surface is cooled down from 2000 K to $\sim$1200 K. We refer to this initial stage (before the heat sink disappears) as the fast cooling stage. Afterwards, the temperature of each CNT segment rises above room temperature, and eventually reaches the same final temperature as the hybrid. After the vanishing of the heat sink region, the temperature decay in the hot surface is much slower. For the same time interval (5 ps to 10 ps), the temperature drops from $\sim$1200 K to $\sim$900 K. Therefore, the existence of the heat sink region in the CNT is very important for heat-dissipation efficiency.

One way to enlarge the heat sink region is to increase the length of the CNT. Figure 3(a) shows the cooling performance of the G-CNT hybrid with a single CNT connection of different lengths. The increase of CNT length progressively reduces the plateau temperature to which the final temperature of the hot surface saturates. Based on the equipartition theorem, the plateau temperature can be estimated as

$$T_{\text{ave}} = \frac{T_H N_H + T_C N_C}{N_H + N_C}, \qquad (1)$$

where T_{H} and T_{C} is the initial temperature of the two hot surfaces and CNT, respectively, and N$_H$ and N$_C$ denote the number of atoms in two hot surfaces and CNT, respectively. The dashed line in figure 3(a) shows the theoretical estimation
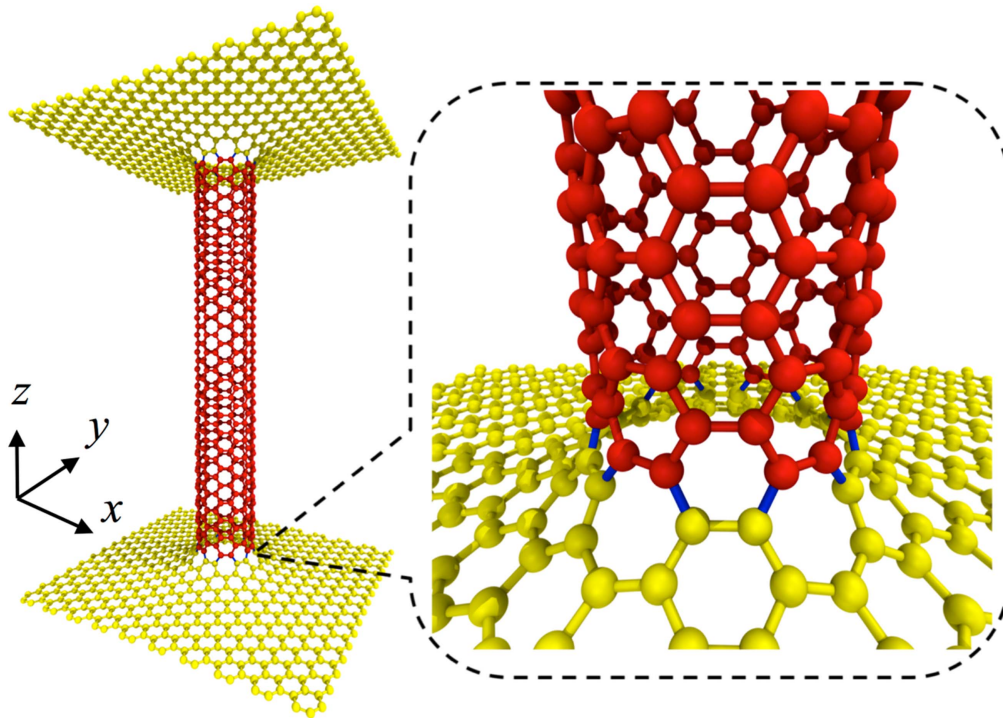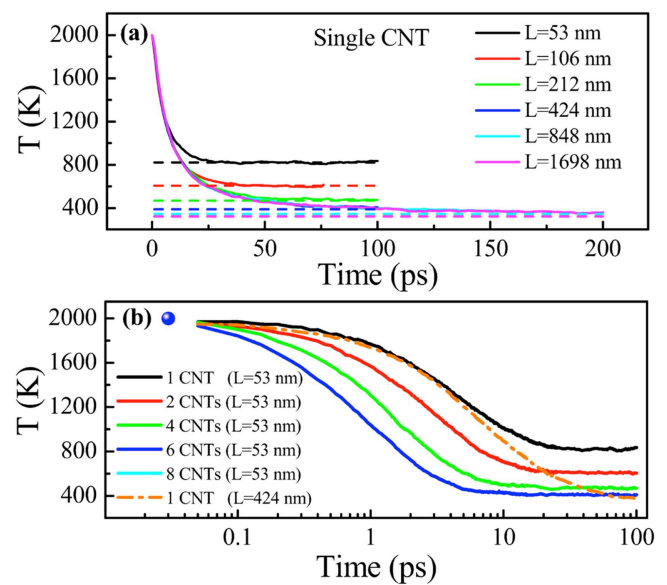
Figure 1. Schematic of the covalently bonded graphene (yellow) and carbon nanotube (red) hybrid structure. The right panel is zoomed in on the graphene-CNT junction seamlessly connected via sp^2 covalent bonding (blue).
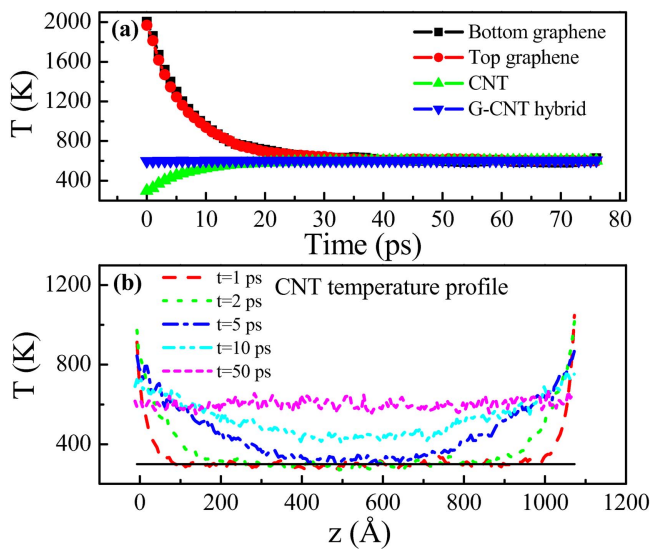
Figure 2. The typical transient cooling process in the G-CNT hybrid. The top and bottom graphene layer is initially at high temperature (2000 K), and the CNT is at room temperature. Here, a single CNT with a length of 106 nm is used in the simulation. (a) Temperature of each component versus time. (b) CNT temperature profile along the length direction. The solid line plots the room temperature for reference.

Figure 3. Cooling high-temperature surface by G-CNT hybrid with different CNT configurations. (a) A single CNT with various lengths. The dashed lines plots the theoretical estimation based on equation (1). (b) Multiple CNTs at the fixed length of 53 nm. The results for the single CNT at L = 53 nm and L = 424 nm are also shown for comparison. The circle denotes the initial temperature of the hot surface.

based on equation (1) at various CNT lengths, which agrees well with the MD simulation results. Moreover, a longer CNT ensures a slightly faster decay of the hot-surface temperature, particularly near the plateau temperature, due to the larger heat sink region (see figures S2–S3). However, the

temperature decay during the first 5 ps is almost the same for various lengths, so the longer CNT cannot significantly improve the performance in the fast cooling stage.

We have shown in a previous study [35] that the *c*-axis thermal conductivity of the G-CNT hybrid increases with the
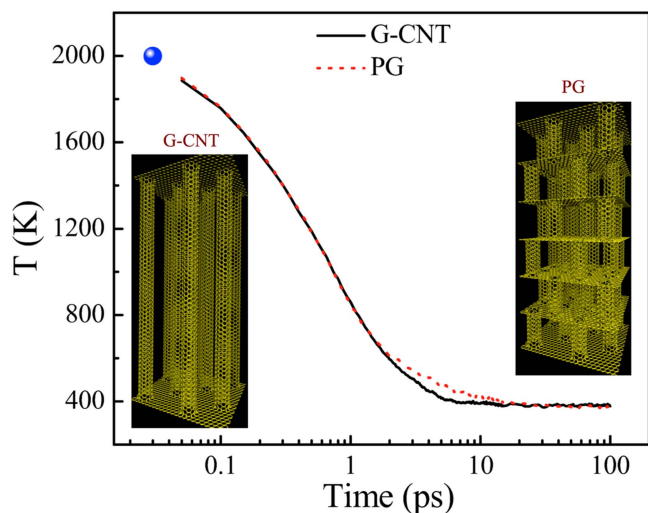
Figure 4. Compare cooling performance between the G-CNT and pillared graphene (PG) structure. The circle denotes the initial temperature of the hot surface. For both structures, the distance between the two hot (top and bottom) surfaces is the same as 53 nm, and there are eight CNT connections in each stack. In the PG structure, six vertical stacks are used.

number of CNT connections, exhibiting an almost linear dependence at low CNT density. Furthermore, Liu *et al* [40] proposed linking two layers of graphene nanoribbons by covalent bonding to the organic molecules. They found the total thermal conductance increases linearly with the number of cross-linkers, indicating independent heat transport channels are established by the covalent bonding. To verify this aspect, we carry out additional transient simulations for G-CNT hybrids with the same CNT length, but various CNT connections arranged in parallel. Compared to the single CNT connection, the parallel connection of multiple CNTs not only brings down the plateau temperature, but also significantly enhances the cooling speed in the fast cooling stage (figure 3(b)), in line with the previous finding for the enhanced thermal conductance with the increasing number of cross-linkers [40]. For instance, compared to a single CNT of length 424 nm, eight CNTs of length 53 nm arranged in parallel provide up to a one order of magnitude speeding up in the cooling of the hot surface. These results are also consistent with the enhanced *c*-axis thermal conductivity calculated from the steady-state simulations[35], providing further proof that parallel heat-dissipation channels are crucial for the high-performance thermal management.

The G-CNT hybrid can be stacked in a vertical direction to form a more complex hybrid structure, known as a 'pillared graphene' (PG) structure [41]. Previous studies found that the PG structure can have enhanced hydrogen storage [41], and efficient heat transfer [42]. To compare the cooling performance, we construct a PG structure of the same CNT density and thickness as that of the G-CNT hybrid, and use the same procedure to simulate the transient cooling process. As shown in figure 4, the hot surface is cooled to the same plateau temperature. However, it takes ∼5 ps and ∼20 ps for the G-CNT and PG structure, respectively, to reach the plateau,

suggesting that the G-CNT structure is more advantageous than the PG structure for efficient heat removal.

Through atomic simulations, Varshney *et al* [42] found that phonon scattering at the CNT-graphene junction is the governing mechanism limiting the thermal transport in the PG system. These junctions are found to cause interfacial thermal resistance, and thus lower the thermal conductivity in the out-of-plane direction [43]. Since the PG structure has many more junctions than the G-CNT (see figure 4), the heat dissipation along the *c*-axis is hindered by these junctions, resulting in a longer cooling time for the PG. Furthermore, the architecture of PG requires that the CNTs from adjacent stacks must be connected to different locations in the graphene layer. As a result, the maximum CNT density in the PG structure is only half of that for the G-CNT structure. We found in a previous study [35] that the *c*-axis thermal conductivity of the G-CNT hybrid is proportional to the CNT density, due to the parallel heat-dissipation channels. Therefore, the G-CNT structure allows for a higher maximum thermal conductivity than the PG structure. Given the simpler architecture and available synthesis techniques [33, 34], we believe the G-CNT structure has a significant advantage over the PG structure for high-performance heat dissipation.

As shown in figure 2, one drawback of the purely solid-state TIM is that the heat stays in the solids, resulting in a constant temperature of the solid matrix, although heat is removed from the hot surface. If the hot surface is repeatedly heated, the average temperature of the solid matrix will keep increasing and eventually saturate to that of the hot surface, thus losing the ability for sustainable cooling. We have demonstrated [35] that liquids can assist the cooling of the solid matrix, and the heat transfer across the solid–liquid interface is limited by Kapitza resistance [44, 45]. The liquid heat sink is a popular cooling option for the high heat-flux electronics [5]. The G-CNT hybrid, when immersed in cold water, establishes an additional heat-dissipation path via the solid–liquid interaction to evacuate the heat from the solid matrix, without affecting the fast heat-dissipation path through the solid matrix [35]. Water is selected as the heat sink media because it has room-temperature thermal conductivity around $0.6 \, \mathrm{W \, m^{-1} \, K^{-1}}$ [46], which is much higher than that of air. To simulate the water reservoir as the heat sink (constant temperature), Langevin thermostat at ambient temperature is applied to all the water molecules during the heat-dissipation process. We have verified that applying thermostat or static flow to the water block has negligible effect on the cooling of the hot surface (see figure S4). In the following, we use a fixed-size G-CNT structure (6 nm × 5 nm × 13 nm with eight CNTs connections), and discuss how to utilize the solid–liquid interaction for efficient heat dissipation.

Figure 5(a) shows the two-dimensional water-density distribution outside the G-CNT hybrid. In contrast to the random molecular orientation in bulk water, the water molecules close to the water–carbon interface exhibit ordered orientation with their dipole normal to the interface [47, 48]. This leads to the so-called layering phenomenon where water molecules near the interface form ordered layers with density
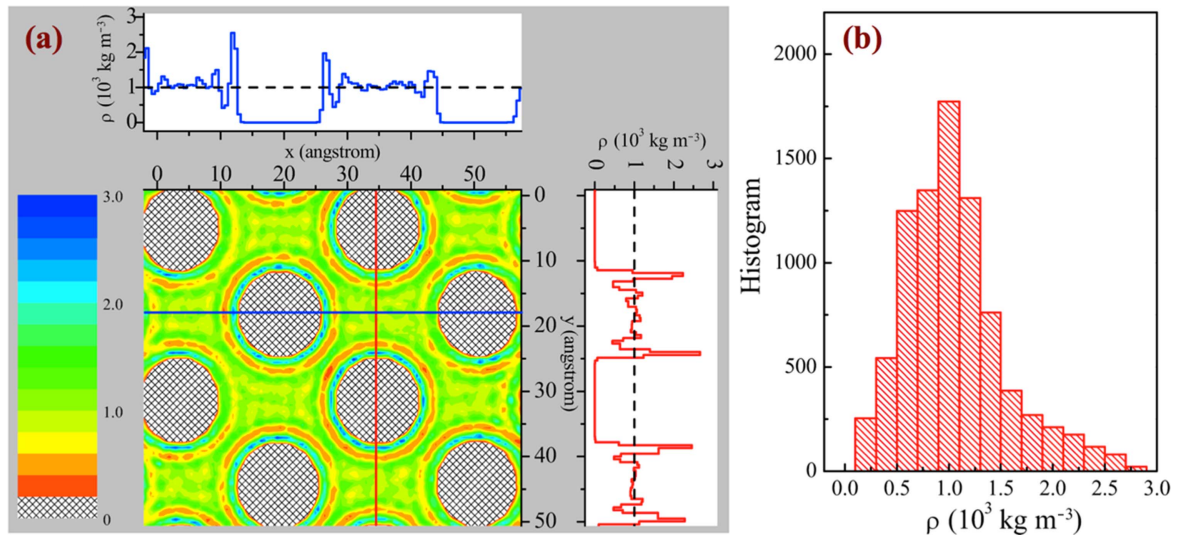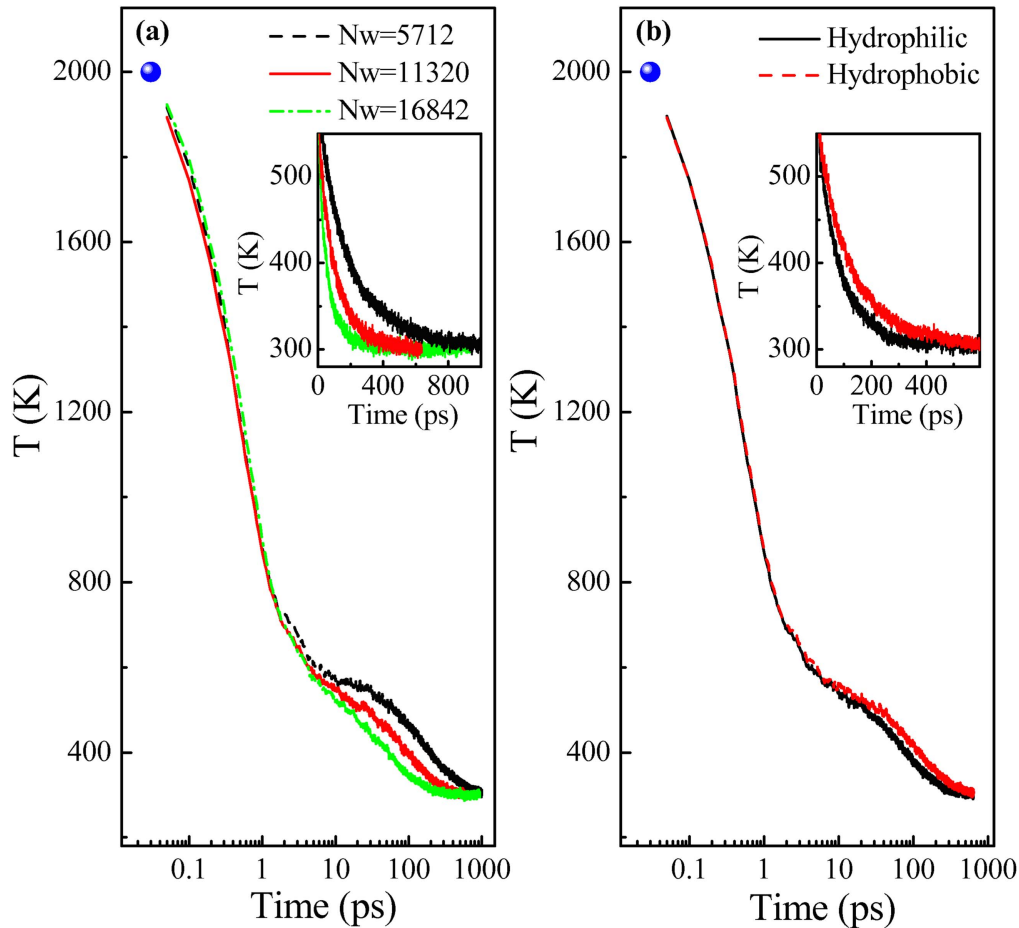
Figure 5. Water density outside the G-CNT hybrid. Here, two graphene sheets have a cross-section of 6 nm × 5 nm, with eight CNTs of length 13 nm connected in between. 11 320 water molecules are used to fill in the space between different CNTs. (a) Two-dimensional water-density distribution. The meshed areas denote the CNT positions. (b) Histogram for the water-density distribution.

oscillations deviating from the bulk water density. In certain interfacial regions, the local water density can reach twice that for the bulk value (figure 5(a)). Away from the interface, the water molecules have no interaction with the interface, thus behaving like bulk water with constant density. We determine how many water molecules are needed to fill in the space between different CNTs under ambient conditions by plotting their statistical density histogram, shown in figure 5(b). The number of water molecules (Nw) is chosen such that the peak of the density histogram is located at the room-temperature bulk water density ($\sim 1.0 \times 10^3$ kg m^{-3}). This requires Nw = 11 320 to fill in the given G-CNT structure.

It has been shown that the Kapitza resistance between the graphene–water interface is inversely proportional to the water-density peak close to the interface [44]. Furthermore, the interfacial water-density peak can be controlled either by applying global pressure or tuning the interfacial wettability (contact angle) [44]. To verify these findings, we carry out two sets of transient cooling simulations. First, we use a fixed contact angle ($\theta = 95°$), but different numbers of water molecules to fill in the space outside the G-CNT hybrid. Given the fixed volume of the G-CNT hybrid, this results in a different overall water-density level, thus changing the interfacial water-density peak. Figure 6(a) shows the cooling performance for different numbers of water molecules. When the G-CNT hybrid is immersed in water, in our previous study [35] we found that there are two kinds of heat-dissipation paths. One path is within the solid matrix (G-CNT hybrid), which leads to the exponential decay of the hot-surface temperature due to the high thermal conductivity of the hybrid, but the heat energy remains inside the solid matrix. The other path is via the solid–liquid interaction, which is a much slower heat-dissipation path compared to the solid–solid path due to the large Kapitza resistance between solid and liquid. Therefore, at the beginning, the heat is dominantly

evacuated through the solid–solid path, causing the same rapid drop in the hot-surface temperature within 1 ps, regardless of the variations in the solid–liquid interaction. After 1 ps, the heat in the solid matrix is dissipated through the solid–liquid path, and the hot-surface temperature starts to deviate for different numbers of water molecules. In our set-up, we find larger water molecules consistently lead to a faster cooling (figure 6(a)). For water molecule number Nw = 5712, Nw = 11 320, and Nw = 16 842, the corresponding decay time to reach the plateau temperature is around 800 ps, 500 ps, and 300 ps, respectively. For the other set of simulations, we fix the number of water molecules (Nw = 11 320) and tune the water contact angle θ at the interface by changing the LJ parameters [39]. As shown in figure 6(b), the decay time is $\sim$300 ps for the hydrophilic interface ($\theta = 29°$), while it is $\sim$600 ps for the hydrophobic interface ($\theta = 140°$). These transient simulation results confirm that pressure and wettability are two independent key factors that can be used to regulate the heat transfer across the solid–liquid interface.

The power density in modern microprocessors exceeds 100 W cm^{-2} on average, and is highly non-uniform across the chip [1]. For this reason, we use graphene to mimic the chip surface in our model, and simulate the chip temperature under constant power input, with and without use of the G-CNT and water for cooling. Without any cooling, the temperature of the graphene surface increases monotonically with time as a consequence of the energy injection, with a faster temperature rise under a larger power density (figure 7(a)). For the largest power density of 10 000 W cm^{-2} considered in this study, the surface temperature increases by 60 K during 1 ns of constant heating. In contrast, when the G-CNT hybrid immersed in water is used for cooling, the temperature of the chip surface can remain at ambient temperature without escalating (figure 7(b)), even for the extremely large power density of

Figure 6. Cooling down of the hot surface by the G-CNT hybrid immersed in water. Here, two graphene sheets have a cross-section of 6 nm × 5 nm, with eight CNTs of length 13 nm connected in between. The circle denotes the initial temperature of the hot surface, and the inset is zoomed in on the slow descending region of temperature. (a) Different numbers of water molecules (N_w) were injected while fixing the water contact angle ($\theta = 95°$). (b) The water wettability was tuned from hydrophilic ($\theta = 29°$) to hydrophobic ($\theta = 140°$) for the fixed number of water molecules ($N_w = 11\,320$).
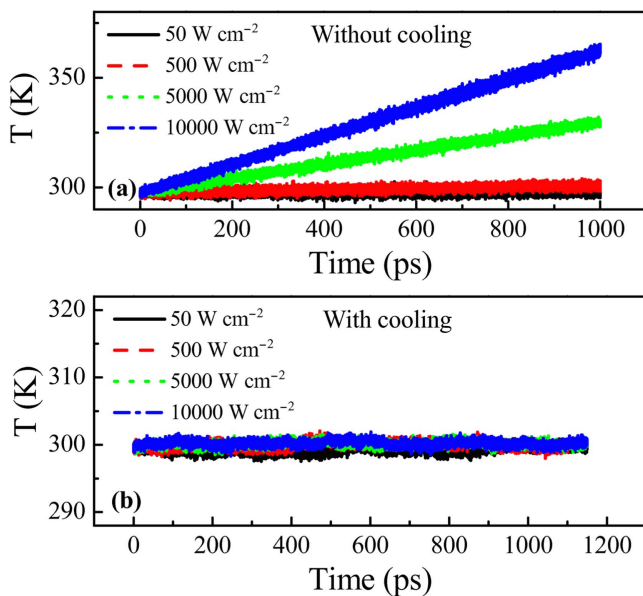
Figure 7. Temperature of the graphene surface subject to the constant power density without (a) and with (b) cooling. Here, the G-CNT hybrid immersed in water is used for cooling. $N_w = 11\,320$ and $\theta = 95°$ are used in this simulation.

$10\,000$ W cm^{-2}. These results demonstrate that the G-CNT hybrid immersed in water is a practical cooling solution for the high heat-flux electronics.

4. Conclusion

In conclusion, we have demonstrated through transient non-equilibrium MD simulations that the G-CNT hybrid is a promising TIM for high-performance cooling applications. Compared to the individual CNT, the G-CNT hybrid has the unique advantage of parallelizing the heat-dissipation capability via CNT arrays while providing a planar contact area for reducing contact thermal resistance, thus significantly speeding up the cooling process. Furthermore, when the G-CNT hybrid is immersed in water, additional heat-dissipation path is established through the solid–liquid interaction, allowing for sustainable cooling of the hot surface. High pressure and hydrophobic interfaces are found to improve the cooling performance. Our study suggests that a G-CNT hybrid immersed in water provides a promising solution for eliminating high flux hotspots in integrated circuit chips.

Acknowledgments

References

[1] Moore A L and Shi L 2014 Emerging challenges and materials for thermal management of electronics *Mater. Today* **17** 163–74

[2] Pop E 2010 Energy dissipation and transport in nanoscale devices *Nano Res.* **3** 147–69

[3] Pop E, Sinha S and Goodson K E 2006 Heat generation and transport in nanometer-scale transistors *Proc. IEEE* **94** 1587–601

[4] Huang W, Rajamani K, Stan M R and Skadron K 2011 Scaling with design constraints: predicting the future of big chips *IEEE Micro* **31** 16–29

[5] Kandlikar S G 2014 Review and projections of integrated cooling systems for three-dimensional integrated circuits *J. Electron. Packaging* **136** 024001

[6] Balandin A A 2011 Thermal properties of graphene and nanostructured carbon materials *Nat. Mater.* **10** 569–81

[7] Xu Y, Li Z and Duan W 2014 Thermal and thermoelectric properties of graphene *Small* **10** 2182–99

[8] Zhang G and Zhang H 2011 Thermal conduction and rectification in few-layer graphene Y junctions *Nanoscale* **3** 4604–7

[9] Ong Z-Y and Pop E 2010 Molecular dynamics simulation of thermal boundary conductance between carbon nanotubes and SiO2 *Phys. Rev.* B **81** 155408

[10] Qiu B and Ruan X 2012 Reduction of spectral phonon relaxation times from suspended to supported graphene *Appl. Phys. Lett.* **100** 193101

[11] Chen J, Zhang G and Li B 2013 Substrate coupling suppresses size dependence of thermal conductivity in supported graphene *Nanoscale* **5** 532–6

[12] Babaei H, Keblinski P and Khodadadi J M 2013 Thermal conductivity enhancement of paraffins by increasing the alignment of molecules through adding CNT/graphene *Int. J. Heat Mass Transfer* **58** 209–16

[13] Fugallo G, Cepellotti A, Paulatto L, Lazzeri M, Marzari N and Mauri F 2014 Thermal conductivity of graphene and graphite: collective excitations and mean free paths *Nano Lett.* **14** 6109–14

[14] Wang J, Zhu L, Chen J, Li B and Thong J T 2013 Suppressing thermal conductivity of suspended tri-layer graphene by gold deposition *Adv. Mater.* **25** 6884–8

[15] Peng X-F and Chen K-Q 2014 Thermal transport for flexural and in-plane phonons in graphene nanoribbons *Carbon* **77** 360–5

[16] Xu X *et al* 2014 Length-dependent thermal conductivity in suspended single-layer graphene *Nat. Commun.* **5** 3689

[17] Li X, Chen J, Yu C and Zhang G 2013 Comparison of isotope effects on thermal conductivity of graphene nanoribbons and carbon nanotubes *Appl. Phys. Lett.* **103** 013111

[18] Wei Z, Yang J, Bi K and Chen Y 2014 Mode dependent lattice thermal conductivity of single layer graphene *J. Appl. Phys.* **116** 153503

[19] Shen Y, Xie G, Wei X, Zhang K, Tang M, Zhong J, Zhang G and Zhang Y-W 2014 Size and boundary scattering controlled contribution of spectral phonons to the thermal conductivity in graphene ribbons *J. Appl. Phys.* **115** 063507

[20] Chen J, Walther J H and Koumoutsakos P 2014 Strain engineering of Kapitza resistance in few-layer graphene *Nano Lett.* **14** 819–25

[21] Liao Q, Liu Z, Liu W, Deng C and Yang N 2015 Extremely high thermal conductivity of aligned carbon nanotube-polyethylene composites *Sci. Rep.* **5** 16543

[22] Kuang Y, Lindsay L and Huang B 2015 Unusual enhancement in intrinsic thermal conductivity of multilayer graphene by tensile strains *Nano Lett.* **15** 6121–7

[23] Xu L Q, Zhang X M and Zheng Y P 2015 Local strain effect on the thermal transport of graphene nanoribbons: a molecular dynamics investigation *PCCP* **17** 12031–40

[24] Sääskilahti K, Oksanen J, Volz S and Tulkki J 2015 Frequency-dependent phonon mean free path in carbon nanotubes from nonequilibrium molecular dynamics *Phys. Rev.* B **91** 115426

[25] Qiu L, Wang X, Su G, Tang D, Zheng X, Zhu J, Wang Z, Norris P M, Bradford P D and Zhu Y 2016 Remarkably enhanced thermal transport based on a flexible horizontally-aligned carbon nanotube array film *Sci. Rep.* **6** 21014

[26] Yang J *et al* 2014 Phonon transport through point contacts between graphitic nanomaterials *Phys. Rev. Lett.* **112** 205901

[27] Shen M, Schelling P K and Keblinski P 2013 Heat transfer mechanism across few-layer graphene by molecular dynamics *Phys. Rev.* B **88** 045444

[28] Cola B A, Xu J, Cheng C, Xu X, Fisher T S and Hu H 2007 Photoacoustic characterization of carbon nanotube array thermal interfaces *J. Appl. Phys.* **101** 054313

[29] Zhang Y, Han H, Wang N, Zhang P, Fu Y, Murugesan M, Edwards M, Jeppson K, Volz S and Liu J 2015 Improved heat spreading performance of functionalized graphene in microelectronic device application *Adv. Funct. Mater.* **25** 4430–5

[30] Li M, Sun Y, Xiao H Y, Hu X J and Yue Y N 2015 High temperature dependence of thermal transport in graphene foam *Nanotechnology* **26** 105703

[31] Hata T, Kawai H, Jono R and Yamashita K 2014 Multi-wall effects on the thermal transport properties of nanotube structures *Nanotechnology* **25** 245703

[32] Wei N, Xu L, Wang H Q and Zheng J C 2011 Strain engineering of thermal conductivity in graphene sheets and nanoribbons: a demonstration of magic flexibility *Nanotechnology* **22** 105705

[33] Kim N D, Li Y, Wang G, Fan X, Jiang J, Li L, Ji Y, Ruan G, Hauge R H and Tour J M 2016 Growth and transfer of seamless 3D graphene-nanotube hybrids *Nano Lett.* **16** 1287–92

[34] Zhu Y *et al* 2012 A seamless three-dimensional carbon nanotube graphene hybrid material *Nat. Commun.* **3** 1225

[35] Chen J, Walther J H and Koumoutsakos P 2015 Covalently bonded graphene-carbon nanotube hybrid for high-performance thermal interfaces *Adv. Funct. Mater.* **25** 7539–45

[36] Plimpton S 1995 Fast parallel algorithms for short-range molecular dynamics *J. Comput. Phys.* **117** 1–19

[37] Lindsay L and Broido D A 2010 Optimized Tersoff and Brenner empirical potential parameters for lattice dynamics and phonon thermal transport in carbon nanotubes and graphene *Phys. Rev.* B **81** 205441

[38] Wu Y, Tepper H L and Voth G A 2006 Flexible simple point-charge water model with improved liquid-state properties *J. Chem. Phys.* **124** 024503

[39] Werder T, Walther J H, Jaffe R L, Halicioglu T and Koumoutsakos P 2003 On the water-carbon interaction for use in molecular dynamics simulations of graphite and carbon nanotubes *J. Phys. Chem.* B **107** 1345–52

[40] Liu X, Zhang G and Zhang Y-W 2014 Thermal conduction across graphene cross-linkers *J. Phys. Chem.* C **118** 12541–7

[41] Dimitrakakis G K, Tylianakis E and Froudakis G E 2008 Pillared graphene: a new 3D network nanostructure for enhanced hydrogen storage *Nano Lett.* **8** 3166–70

[42] Varshney V, Patnaik S S, Roy A K, Froudakis G and Farmer B L 2010 Modeling of thermal transport in pillared-graphene architectures *ACS Nano* **4** 1153–61

[43] Park J and Prakash V 2014 Phonon scattering and thermal conductivity of pillared graphene structures with carbon nanotube-graphene intramolecular junctions *J. Appl. Phys.* **116** 014303

[44] Alexeev D, Chen J, Walther J H, Giapis K P, Angelikopoulos P and Koumoutsakos P 2015 Kapitza resistance between few-layer graphene and water: liquid layering effects *Nano Lett.* **15** 5744–9

[45] Ramiere A, Volz S and Amrit J 2016 Thermal resistance at a solid/superfluid helium interface *Nat. Mater.* **15** 512–6

[46] Ramires M L V, Decastro C A N, Nagasaka Y, Nagashima A, Assael M J and Wakeham W A 1995 Standard reference data for the thermal conductivity of water *J. Phys. Chem. Ref. Data* **24** 1377–81

[47] Walther J H, Jaffe R, Halicioglu T and Koumoutsakos P 2001 Carbon nanotubes in water: structural characteristics and energetics *J. Phys. Chem.* B **105** 9980–7

[48] Jaffe R L, Gonnet P, Werder T, Walther J H and Koumoutsakos P 2004 Water–carbon interactions 2: calibration of potentials using contact angle data for different interaction models *Mol. Simul.* **30** 205–16